ORIGINAL ARTICLE

Antidiabetic potentials of green-synthesized alpha iron oxide nanoparticles using stem extract of *Securidaca longipedunculata*

Augustine Innalegwu Daniel[1] · Maimuna Bello Umar[1] · Oladejo Jimoh Tijani[2] · Rukayya Muhammad[1]

Abstract

The study evaluated the antidiabetic potentials of green-synthesized iron oxide (Fe_2O_3) nanoparticles using stem extract of *Securidaca longipedunculata*. Fe_2O_3 nanoparticles were synthesized via green route and characterized using different analytical tools. Diabetes was induced in albino Wister rats by a single dose intraperitoneal injection of 90 mg/kg bodyweight of alloxan monohydrate and treated for 21 days. Lipid profiles, biochemical parameters and histopathological study of the liver and kidney were also examined. The characterization results confirmed formation of spherical, hematite phase of iron oxide with crystallite size of 4.07 nm and maximum wavelength of 372.27 nm. There was a significant ($p < 0.05$) decrease in blood glucose level of the diabetic rats from 409.50 ± 5.50 to 199.1550 ± 9.33 mg/dL in Fe_2O_3 nanoparticle group compared to the diabetic and extract control groups. Group treated with Fe_2O_3 nanoparticle shows an increase in bodyweight throughout the treatment period and is significantly different ($p < 0.05$) with the other groups. There is a significant difference ($p < 0.05$) in serum alanine transaminase (ALT), aspartate transaminase (AST) and alanine phosphatase (ALP) of the Fe_2O_3 nanoparticles treated group with Glibenclamide and diabetic control group. The histopathology of the liver and kidney shows normal histoarchitecture with no features of acute or chronic damage in all groups. The green-synthesized Fe_2O_3 nanoparticles have the potential of treating hyperglycemia and could serve as drug lead in the treatment of diabetes.

Keywords Diabetes · Green synthesis · Iron oxide nanoparticles · Histopathology · Alloxan monohydrate

Introduction

Diabetes mellitus (DM) is a metabolic disorder caused by abnormalities in insulin secretion, insulin action, or both [1]. It is characterized by persistent hyperglycemia and problems in carbohydrate, lipid, and protein metabolism. Long-term damage is one of the outcomes of diabetes mellitus with diverse organ malfunction and failure [1]. There are three forms of diabetes mellitus; type 1 diabetes (insulin-dependent diabetes mellitus) is an autoimmune disease that occurs when the β-cells of the pancreas are damaged, resulting in the pancreas producing little or no insulin. It most commonly affects children and young adults [2]. Type 2 diabetes, commonly known as "insulin-dependent diabetes mellitus," is

the most common type of diabetes in adults, accounting for more than 90% of cases. Insulin resistance is a condition in which the pancreas generates enough insulin but the body is unable to use the insulin efficiently [1, 2]. The third form of diabetes is the gestational diabetes mellitus (GDM) which is a type of glucose intolerance that develops or is first noticed during the second or third trimester of pregnancy. The use of synthetic oral hypoglycemic medications and insulin in the treatment of diabetes is common. They are, however, costly, have substantial side effects, and require daily dosing [1].

Nanotechnology's global market has risen at an exponential rate in recent years as a result of its widespread applicability in a various of fields [3]. This qualifies nanomaterials as a novel solution to a variety of challenges in healthcare, materials, energy storage, catalysis, and other fields [3]. There are three forms of iron oxide nanoparticles utilized as drug carriers currently: magnetite (Fe_3O_4), maghemite (γ-Fe_2O_3), and hematite (α-Fe_2O_3) [4, 5]. All of these iron oxides have distinct characteristics such as low toxicity, biocompatibility, and stability [6]. They have the potential to be used as magnetic resonance imaging (MRI) agents as well as routine

✉ Augustine Innalegwu Daniel
   a.daniel@futminna.edu.ng

1   Department of Biochemistry, Federal University of Technology, P.M.B 65, Minna, Niger, Nigeria

2   Department of Chemistry, Federal University of Technology, P.M.B 65, Minna, Niger, Nigeria

✆ Springer

diagnostic instruments [7, 8]. Heavy metals, dyes, and bacteria have all been reported to be removed from water using iron oxide nanoparticles, as well as biomedical applications such as site-specific drug delivery and tumor cell [9, 10]. Iron-based nanoparticles have also been shown to be effective against a number of pathogenic bacterial strains and fungi due to their ability to produce highly reactive oxygen species (ROS) [11].

Sol–gel, chemical reduction, co-precipitation, and hydrothermal synthesis are some of the processes used for the synthesis of nanomaterials [12]. However, there is a pattern switched to new, less expensive, and safer techniques to synthesize nanoparticles, resulting in a novel, affordable and safer method to synthesize nanoparticles reulting in a sustainable ecofriendly concept such as green nanoparticles [13, 14]. In green or biosynthesis, nanoparticles are synthesized using biological resources such as bacteria, fungus, algae, or plants [15–17]. Physical and chemical methods of synthesis on the other hand are also employed, although they have drawbacks such as the generation of toxic waste, as illustrated by the use of toxic substances in chemical synthesis [18, 19].

Metals are important in a variety of metabolic pathways including glucose metabolism [1]. Nanoparticles synthesized from the oxide of zinc, silver, gold, and core–shell have all been reported to have antidiabetic properties [20, 21]. Furthermore, Sharifi et al. [22] discovered that in human primary adipocytes, α-Fe_2O_3 nanoparticles suppress genes involved in the development of T2DM.

Securidaca longipedunculata commonly known by its vernacular name as "king of medicines", violet tree, fiber tree or Rhodesian violet in English, Uwar magunguna or Sanya in Hausa and Ipeta in Yoruba is found in most tropical and Sub-Saharan African [23]. The leaves, stem and root if the plant has been reported to be used for the treatment of various ailments such as sexually transmitted disease, fungal infection, diabetes, wounds [24], malaria and tuberculosis [25]. The plant has been reported to contain useful bioactive compounds such as xanthones, flavonoids, terpenes, coumarins and steroids [26]. Hence, this research was focused on the evaluation of the antidiabetic potentials of green-synthesized α-Fe_2O_3 nanoparticles in alloxan-induced diabetic rats. The green-synthesized nanoparticle was characterized using different analytical tools and the antidiabetic potentials of the nanoparticle was evaluated in alloxan-induced diabetic rats.

Materials and methods

Chemicals

Analytical grade ferric nitrate nonahydrate $(Fe(NO_3)_3 \cdot 9H_2O))$ (99.99%), Sodium hydroxide pellets (NaOH) (80%) were purchased from Merck, India. All chemicals are used without further purification.

Collection and preparation plant extract

The stems of *Securidaca longipedunculata* were collected from the environment of Federal University of Technology Minna, Nigeria. The stems were washed several times with distilled water and air dried for 4 weeks at the Biochemistry Laboratory. The dried stems were chopped into pieces and pulverized into fine powder using mortar and pestle. Twenty grams (20 g) of fine powder was boiled with 100 mL of deionized water at 80 °C for 30 min and the extract was then filtered Whatman No. 1 filter paper to obtain the filtrate.

Quantitative phytochemical analysis of *Securidaca longipedunculata* extract
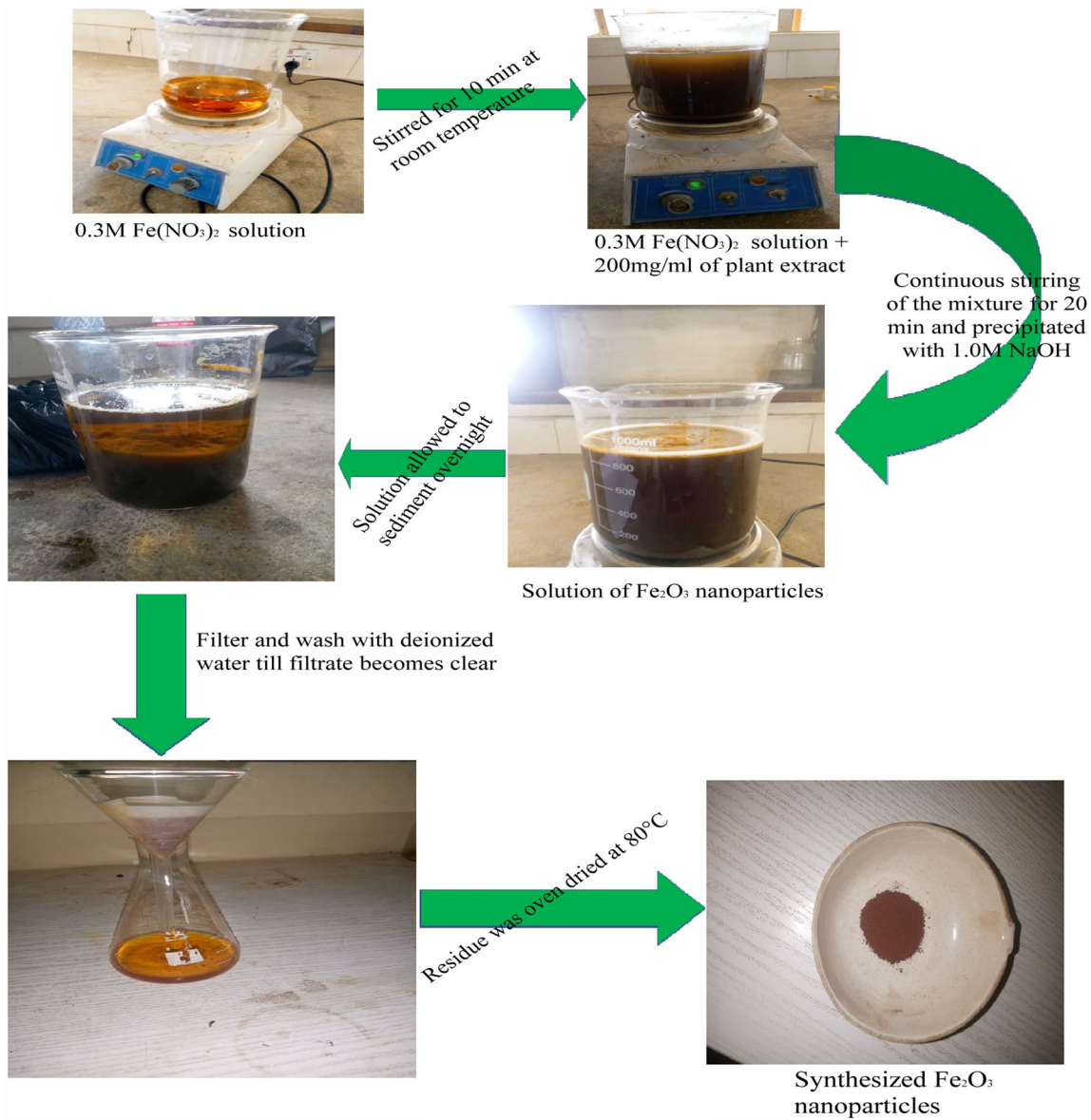
Determination of total flavonoids

Aluminum chloride ($AlCl_3$) Colorimetric method was used for the determination of flavonoid content [27]. An aliquot of the plant extract (0.5 mL) was mixed with 1.5 mL of methanol, 0.1 mL of 10% $AlCl_3$ (w/v), 0.1 mL of 1 M sodium acetate and 2.8 mL of distilled water and allowed to stand at ambient temperature for half an hour. Quercetin solutions at concentrations of 12.5–100 g/mL in methanol was used for the calibration of the standard curve. Absorbance of the mixture and the standard were read at 415 nm.

Determination of total phenols

Folin–Ciocalteau spectrophotometric method was used for the determination of total phenolic content of the extract [28]. An aliquot of the plant extract (0.5 mL) was mixed with 2.5 mL of 10% Folins reagent and 2 mL of 7.5% sodium carbonate, mixed properly and incubated for 40 min at 45 °C. Absorbance of the mixture was read at 765 nm. The total phenolic content of the extract was extrapolated form Gallic acid standard curve.

Determination of total tannins

The tannic acid content of the extract was extrapolated from the tannic acid standard curve [29]. 0.2 g of the plant sample was weighed into a 50 mL beaker containing 20 mL of 50% methanol, covered with parafilm and heated in a water bath at 80 °C for 1 h. The contents of the mixture were transferred into a 100 mL volumetric flask after being thoroughly shaken. Approximately 20 mL of distilled water, 2.5 mL Folins reagent and 10 mL 17% Na_2CO_3 were added and mixed properly before allowing to stand for 20 min. After color development, the absorbance of tannic acid standard

0.3M Fe(NO₃)₂ solution

Stirred for 10 min at room temperature

0.3M Fe(NO₃)₂ solution + 200mg/ml of plant extract

Continuous stirring of the mixture for 20 min and precipitated with 1.0M NaOH

Solution allowed to sediment overnight

Solution of Fe₂O₃ nanoparticles

Filter and wash with deionized water till filtrate becomes clear

Residue was oven dried at 80°C

Synthesized Fe₂O₃ nanoparticles

Flow chat of the processes for green synthesizes of α-Fe$_2$O$_3$ nanoparticles

solution and sample was measured with a spectrophotometer at 760 nm.

Green synthesis of Fe$_2$O$_3$ nanoparticles

Ferric nitrate nonahydrate (Fe(NO$_3$)$_3$·9H$_2$O)) was used as the precursor for the synthesis of the α-Fe$_2$O$_3$ nanoparticles. 200 mL of 0.3 M ferric nitrate solution was stirred for 10 min at room 25 °C on magnetic stirrer before adding 100 mL of *S. longipedunculata* stem extract and the mixture were stirred further for another 20 min at room temperature. Sodium hydroxide (1 M) was added dropwise to adjust the pH from acidic to basic and precipitate a brown color α-Fe$_2$O$_3$ nanoparticles and the solution was allowed to stand overnight to sediment [30]. The solution was decanted, filtered and washed severally with deionized water until a clear filtrate was obtained which was dried in a hot air oven at 80 °C for 3 h. The step-by-step synthesis of α-Fe$_2$O$_3$ nanoparticle is shown in the flow chart below.

Characterization of Fe$_2$O$_3$ nanoparticles

The absorption band of the synthesized α-Fe$_2$O$_3$ nanoparticles were characterized using a double beam UV–visible spectrophotometer (Shimadzu UV-1800) at a wavelength range of 200–800 nm, Energy-dispersive X-ray spectroscopy (EDX) (Zeiss Aunga), high-resolution transmission electron microscopy (HRTEM) (Zeiss Aunga), high-resolution scanning electron microscope (HRSEM) (Zeiss Aunga) and X-ray diffraction (XRD) (Bruker d8) to confirm the synthesis of the elemental composition, morphology, dispersity and crystallinity of the Fe$_2$O$_3$ nanoparticles.

Experimental animals/ethics

Thirty (30) Wistar rats of both sexes weighing between 100–150 g were purchased from the animal farm of the University of Jos, Jos, Plateau State, Nigeria. The rats were kept in well-ventilated metal cages and maintained at room temperature of 28 ± 2 °C, 45–55% of relative humidity on a 12 h light/12 h dark cycle, with access to water and pelletized standard guinea feed ad libitum. The rats were kept for 2 weeks to acclimatize to environmental conditions.

Induction of diabetes mellitus

Diabetes mellitus (DM) was induced in the rats by a single intraperitoneal (i.p.) injection of 90 mg/kgbwt of alloxan monohydrate (Sigma, St. Louis, USA) in PBS (pH = 7.4) [31]. Animals with fasting plasma glucose concentration (FPGC) > 111 mg/dL, measured using Fine test Auto-coding Premium Blood Glucose Monitoring System for self-testing, for 5 consecutive days were considered diabetic and selected for the study. A total of thirty (30) Wistar rats of both sexes were divided into 5 groups of 6 rats each. The animals were deprived of food and water for additional 16 h before commencement of treatment [31]. All procedures were conducted in accordance with the guidelines for the care and use of laboratory animals (USA National Institute of Health Publication No. 80-23, revised 1996) and were reviewed and approved by the Animal Ethics Committee of Federal University of Technology Minna, Nigeria.

Experimental design

The rat groups were assigned on the basis of treatments received by oral gavage on daily basis for 21 days as follows: group I: normal control rats received 1.0 mL/kgbwt of PBS, group II: diabetic rats received 5 mg/kgbwt of glibenclamide (standard drug), group III: diabetic control rats, group IV: diabetic rats treated with 300 mg/kgbwt of methanol extract of *S. longipedunculata*, group V: diabetic rats treated with 300 mg/kgbwt of Fe$_2$O$_3$_NPs.

The body weight of rats in each group was also determine on every 7 days interval.

Collection and preparation of blood and tissues

On the 21st day of the experiment, overnight fasted rats were euthanized using 150 mg/kgbwt of sodium pentobarbitone anesthesia and blood samples were collected via cardiac puncture from each mouse into a plain sample bottle. The blood samples were kept at room temperature for 2 h to coagulate and then centrifuged at 2000 rpm for 10 min then serum was separated with clean Pasteur pipette and stored frozen until used for biochemical analyses. The liver and kidney of rats were excised, rinsed in normal saline and preserved in 10% formalin (v/v) for histopathological study [32].

Biochemical assays

The biochemical parameters of rats at the end of 21 days treatment with the extract were determined using assay kits. High density lipoprotein (HDL), alanine aminotransferase (ALT), alkaline phosphatase (ALP) and aspartate aminotransferase (AST) were determined following the procedure described in the reagent kits manual (AGAPPE Diagnostics Ltd., Switzerland). Total cholesterol (TC) and triglyceride concentrations (TRIG) were determined following the procedure outline in the reagent kits manuals

(TECO Diagnostics Ltd., USA). Additionally, serum LDL-C concentration was determined according to the formula described by Friedewald [33] and reported Oluba et al. [34].

$$[LDL - C] = [TC] - [HDL - C] - \frac{TAG}{5} \qquad (1)$$

Serum VLDL-C concentration was estimated using the methods of Burnstein and Sammaille, [35] where the ratio of serum VLDL-C to triglyceride concentrations was fixed at 1:5 in fasting animals.

$$[VLDL - C] = \frac{TAG}{5} \qquad (2)$$

Statistical and data analyses

Data were expressed as mean ± standard error of the mean. Data were expressed as mean ± standard error of the mean. Means of all parameters among groups and within a group were compared using one-way ANOVA followed by Duncan's post hoc multiple comparison test. Values of $p < 0.05$ were considered statistically significant. SPSS Version 20 software (IBM Corporation, Armonk, NY, USA) and Origin software version 9.55 OriginPro 2018 (64-bit) SR1 b9.5.1.195 were used for statistical analysis.

Results and discussion

Stem extract of *S. longipedunculata* contain phenols, flavonoids and tannins in various amounts (Table 1). These phytochemicals have been reported to act as a reducing and stabilizing agent for the synthesis of nanoparticle [36]. According to Ovais et al. [3], the presence of nucleophilic aromatic ring and the hydroxyl functional groups present in these phytochemicals enables them to act as metal-chelators hence stabilizing the synthesis of metal nanoparticles. Hence, the presence of these phytochemicals in sufficient amount in *S. longipedunculata* makes it a good candidate for the synthesis of α-Fe₂O₃ nanoparticles. The interaction of phytochemicals presents in the plant extract with the metal precursor resulted in the development of a reddish-brown

Table 1 Quantitative phytochemical contents of methanol extract of *S. longipedunculata*

Phytochemicals	Amounts (mg/100 g)
Phenols	201.62 ± 1.98
Flavonoids	49.820.63
Tannins	114.25 ± 3.71

Values are expressed in Mean ± standard error of mean of triplicate determination

precipitate leading to the formation of α-Fe₂O₃ nanoparticles [36]. The homogeneous mixture of iron salt and the plant extract at room temperature could not convert Fe^{3+} to Fe^0 but the interaction of the phytochemicals with ions of the iron to form α-Fe₂O₃ nanoparticles due to its susceptibility to oxidation [36].

The optical properties of the nanoparticles was confirmed by UV–visible analysis (Fig. 1a). The maximum absorption spectrum (λ_{max}) of the synthesized nanoparticles was observed at 372.27 nm which is in line with the report of Bibi et al. [30], and Behera et al. [37] who independently reported the λ_{max} of 371.71 nm. Further confirmation of the synthesized of α-Fe₂O₃ nanoparticles was carried out using the energy dispersive X-ray analysis (EDX) (Fig. 1b). The EDX result of the green-synthesized α-Fe₂O₃ nanoparticles shows that it consists of majorly Fe and O in the ratio of 2:1. The spectrum shows a broad and intense peak belonging to Fe and O and a trace of C with a relative abundance of 72.61, 23.89 and 3.50% respectively. The source of the carbon maybe from the phytochemical constituents of the extract such as phenols, flavonoids and tannins which are present in the extract [30]. The crystal formation of the synthesized α-Fe₂O₃ nanoparticles was determined using the X-ray diffraction (XRD) analysis (Fig. 1c). The XRD pattern of α-Fe₂O₃ nanoparticles revealed the spheroidal structured hematite of the nanoparticles with peaks at 2θ values of 24.14°, 33.15°, 35.61°, 40.86°, 49.48°, 54.09°, 57.59°, 62.45° and 63.99° corresponding to diffraction planes of (012), (104), (110), (113), (024), (116), (018), (214) and (300) respectively which matches with the JCPDS-33-0664 [38]. This assigned to the characteristic structure of pure α-Fe₂O₃ crystal with a rhombohedrally centered hexagonal structure [38]. The intense and sharp peaks confirmed that the synthesized α-Fe₂O₃ nanoparticles using extract of *S. longipedunculata* are crystalline in nature [39–41]. The mean crystallite size was found to be 4.07 nm using the Debye–Scherrer equation. This agreed with the report of Bhuiyan et al. [36] who reported a crystalline size of 4.58 nm.

The morphology of the synthesized nanoparticle shown in Fig. 2a indicated that the synthesized nanoparticles are agglomerated spherical particles of different sizes. The large agglomerated clusters were formed as a result of the accumulation of tiny blocks of various bioactive reducing agents in the plant extract or it could be due to the ability of iron-based nanoparticles to agglomerate due to magnetic interactions [36].

High resolution transmission electron microscope (HRTEM) of the nanoparticles revealed the spheroidal shape of the nanoparticle which may be due to the magnetic nature of iron with size in the range of 25–45 nm (Fig. 2b). The high-resolution TEM image and the selected area electron diffraction (SAED) pattern (Fig. 2c) acquired from an
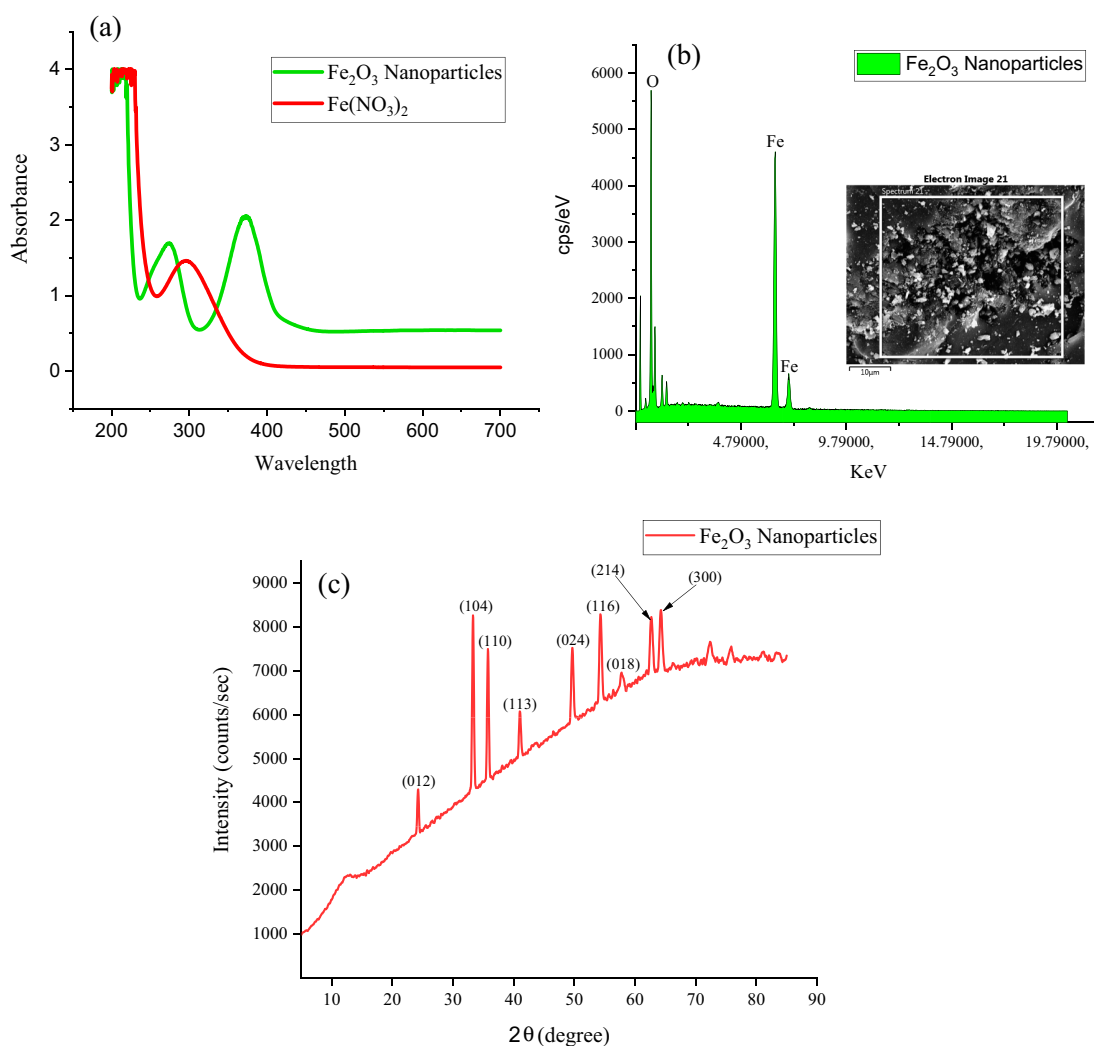
Fig. 1 **a** UV–Vis spectrum, **b** elemental composition and **c** X-ray diffraction pattern of green-synthesized α-Fe$_2$O$_3$ nanoparticles using stem extract of *S. longipedunculata*

area containing a large number of nanoparticles in keeping with the XRD data. The rings in the SAED pattern can be indexed as the cubic hematite reflections (102), (104), (110) and (006).

Fasting blood glucose (FBG) level of alloxan-induced diabetic rats was monitored for all studied groups during the experiment time (21 days) as shown in Fig. 3. The diabetic control group had a significant higher ($p < 0.05$) FBG level (548.10 ± 4.33 mg/dL) than the normal control group (89.50 ± 2.66 mg/dL) on day 12 before the death of rats in the diabetic control group. The level of FBG level in Glibenclamide treated group was decreasing with time. After the first day of treatment (day 6), the FBG level was 160.00 ± 38.00 mg/dL which is significantly lower ($p < 0.05$) than the diabetic control group (575.33 ± 6.54 mg/dL). There was no significant difference ($p > 0.05$) between the group

treated with 300 mg/kgbwt of *Securidaca longipedunculata* extract and Fe$_2$O$_3$ nanoparticle after the first day of the treatment. At day 21, the FBG level of Glibenclamide treated group was 70.50 ± 5.50 mg/dL which was significantly lower than the nanoparticle treated group (199.15 ± 9.33 mg/dL), the extract treated group (212.50 ± 3.50 mg/dL) and the normal control group (81.00 ± 2.11 mg/dL). Rats in the diabetic control group could not survive till day 21 because of the elevation of the blood glucose beyond the normal tolerable level. The result of this study is consistent with the report of Lamiaa et al. [42] who also reported the role of superparamagnetic α-Fe$_2$O$_3$ nanoparticle in reducing the blood glucose of diabetic rats. Studies have also shown that iron metabolism indicators (transferrin, ferritin, hepcidin, transferrin receptor and so on) can directly or indirectly affect the occurrence and development of type 2 diabetes [43]. The
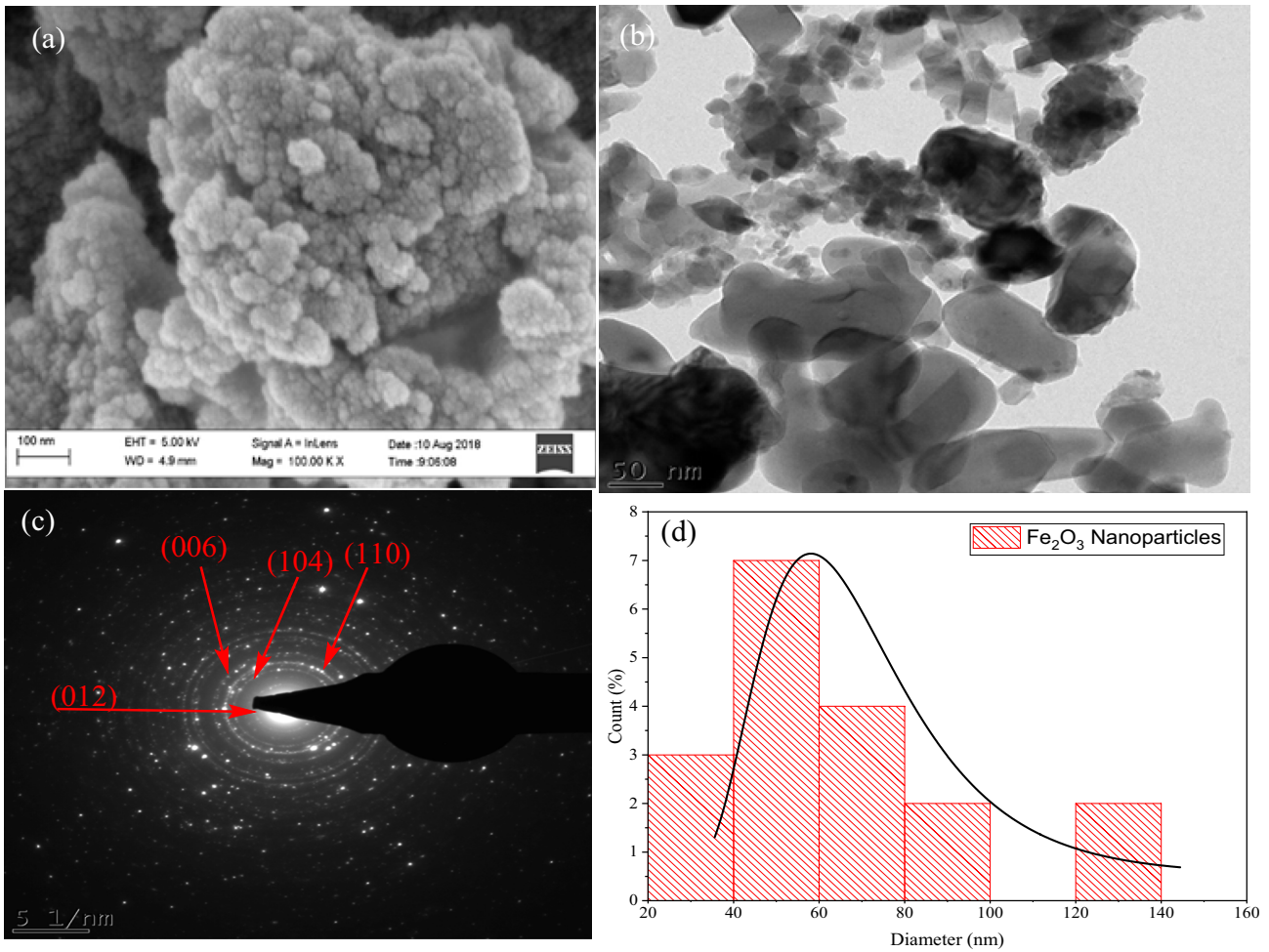
Fig. 2 **a** Scanning electron microscopy image, **b** high-resolution transmission electron microscopy image, **c** selected area electron diffraction patterns and **d** particle size distribution of green-synthesized α-Fe_2O_3 nanoparticles using stem extract of *S. longipedunculata*

Fig. 3 Hypoglycemic effects of green-synthesized α-Fe_2O_3 nanoparticles on fasting blood glucose level of alloxan-induced diabetic rats
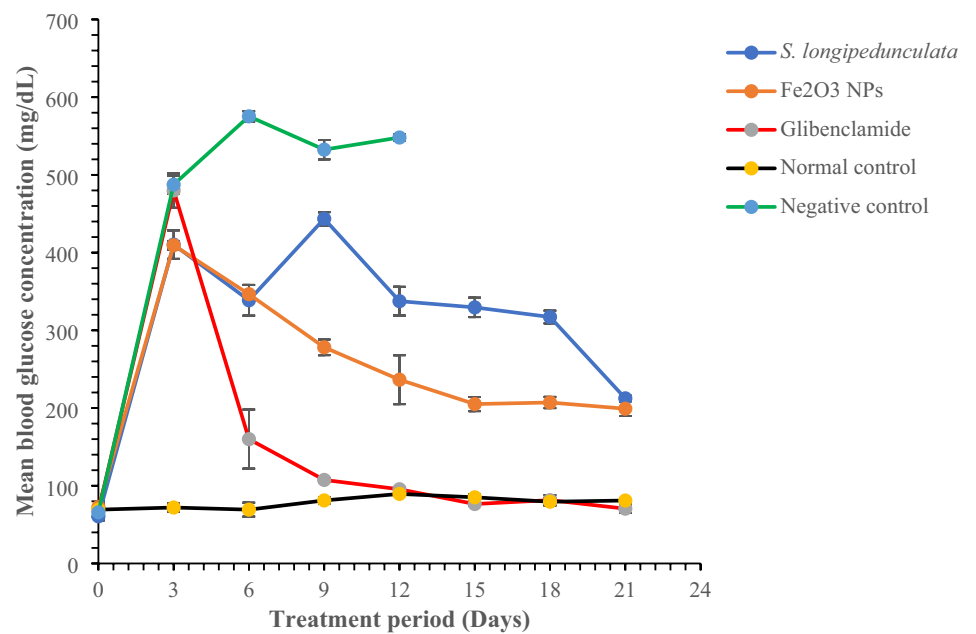
study also shows that α-Fe_2O_3 nanoparticle could increase serum insulin in diabetic rat treated with the nanoparticle compared with group treated with Glibenclamide. There are few studies that have investigated the therapeutic effect of α-Fe_2O_3 nanoparticle on insulin levels or secretion. However, others have demonstrated that iron overload regulates insulin production in pancreatic β-cells and is thought to contribute critically to impair glucose metabolism in diabetic patients [44]. However, in this study, 300 mg/kg bodyweight of α-Fe_2O_3 nanoparticles significantly lowered blood glucose level from 409.50 ± 5.50 to 199.1550 ± 9.33 mg/dL on the 21st day of treatment compared with the diabetic and extract control groups indicating that there was no overload of the nanoparticle that could alter the function of the pancreatic β-cells as previously reported by other authors. Flavonoids and glycosides coated metallic oxide nanoparticles have been reported to induce the inhibition of dipeptidyl peptidase IV (DPPIV)-a protease enzymes which inhibit glucagon-like peptide-1 (GLP-1) and glucose-dependent insulinotropic polypeptide (GIP) receptor resulting in an increase in secretion of insulin from pancreatic β-cells. Also, terpenoids and flavonoids coated metallic nanoparticles inhibit protein tyrosine phosphatase 1B (PTP-1B) enzyme present on the endoplasmic reticulum membrane and result in the stimulation of insulin signaling pathways and ultimately glucose uptake in adipocytes and muscle cells. Finally, metallic oxide nanoparticles inhibit α-amylase and α-glucosidase which reduces the release of glucose [45, 46].

Hence, the presence of phytochemicals such as flavonoids, phenols and tannins in the extract of *S. longipedunculata* may have enhanced the antidiabetic potentials of α-Fe_2O_3 nanoparticles observed in this study.

Diabetes is often characterized by weight loss due to breakdown of body tissues. There was a significant weight reduction ($p < 0.05$) in group treated with α-Fe_2O_3 nanoparticles compared with the normal control group and the extract treated group (Fig. 4). This report supports the findings of Najafabadi et al. [47] who reported a weight loss from the treatment of rats with 50 and 100 mg/kg bodyweight per day of Fe_2O_3 nanoparticles. In another report by Szalay et al. [48] and Zhu et al. [49], rats injected with 1 and 5 mg/kg α-Fe_2O_3 nanoparticles for 14 days showed a significant weight reduction in their bodyweight. This observation could be attributed to the role of iron in initiating oxidative stress [47]. Reactive oxygen species (ROS) maybe produced by α-Fe_2O_3 nanoparticles leading to the generation of hydroxyl radicals and super hydroxide hydrogen. Subsequently, this process may lead to apoptosis or cell death [50]. Furthermore, the decrease in bodyweight of the animals may be attributed to the role of α-Fe_2O_3 nanoparticles in reducing superoxide dismutase and glutathione enzymes [51]. These enzymes play a significant role in reducing of the ROS [47].

Despite the documented antidiabetic potentials of α-Fe_2O_3 nanoparticles in this study, the effect of nanoparticles on hepatorenal toxicities are of great concerns. The present study shows that the treatment of alloxan-induced

Fig. 4 Effects of green-synthesized Fe_2O_3 nanoparticles on the mean bodyweight of alloxan-induced diabetic rats
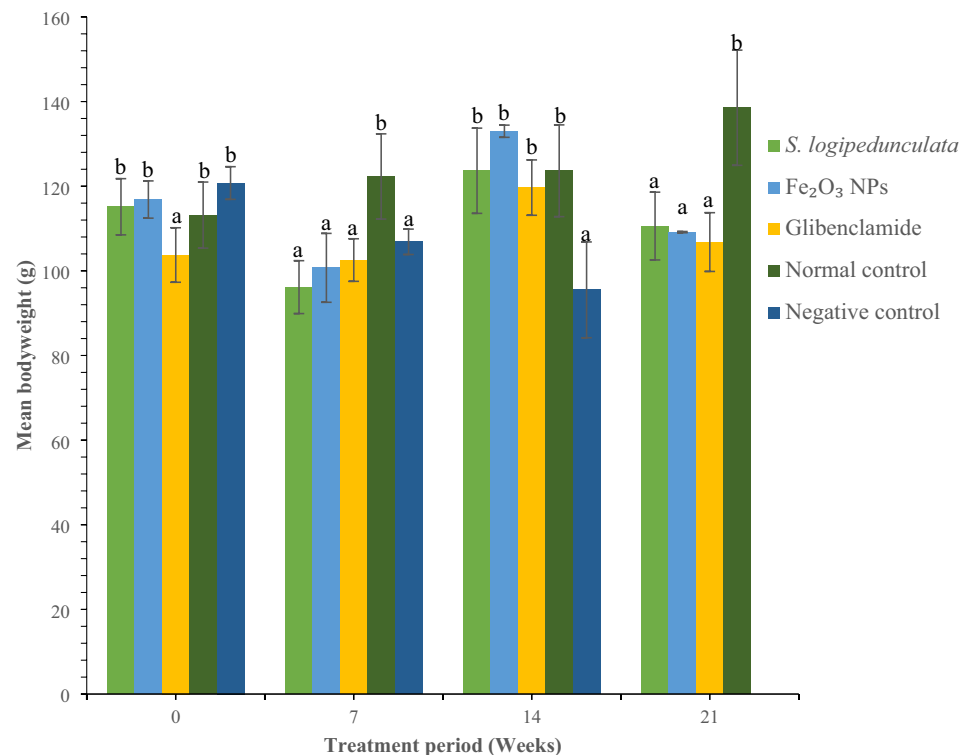
Table 2 Effect of green-synthesized α-Fe$_2$O$_3$ nanoparticles on serum enzymes and lipid profiles of alloxan-induced diabetic rats

Groups	ALT (U/L)	AST (U/L)	ALP (U/L)	TC (mg/dL)	TRIG (mg/dL)	HDL(mg/dL)	LDL (mg/dL)	VLDL(mg/dL)
SL 300	28.03 ± 3.60[a]	39.44 ± 3.38[b]	101.92 ± 10.60[a]	270.38 ± 4.44[b]	119.71 ± 3.84[c]	72.70 ± 0.34[c]	173.74 ± 4.87[b]	23.94 ± 0.77[b]
Fe$_2$O$_3$-NPs	24.68 ± 4.16[a]	63.30 ± 5.71[c]	101.14 ± 2.30[a]	239.89 ± 2.95[a]	92.60 ± 3.04[a]	91.32 ± 2.89[d]	130.05 ± 5.23[a]	18.52 ± 0.61[a]
Glibencla-mide	28.63 ± 6.77[a]	98.63 ± 10.23[d]	102.11 ± 12.32[a]	254.03 ± 4.25[b]	124.74 ± 9.66[c]	91.41 ± 4.88[d]	137.67 ± 2.50[a]	24.95 ± 3.10[c]
Normal control	32.78 ± 3.15[b]	22.77 ± 1.83[a]	114.59 ± 4.00[b]	283.42 ± 3.69[c]	108.44 ± 3.00[b]	67.12 ± 2.00[b]	194.61 ± 6.29[b]	21.69 ± 0.60[b]
Negative control	56.56 ± 7.66[c]	39.45 ± 1.25[b]	134.03 ± 13.33[c]	318.34 ± 2.46[d]	122.92 ± 6.55[d]	56.36 ± 9.00[a]	237.40 ± 7.32[d]	24.58 ± 11.21[c]

Values are expressed in mean ± standard error of mean of quadruplet determination. Values with the same superscript on the same row have no significant difference at $p > 0.05$

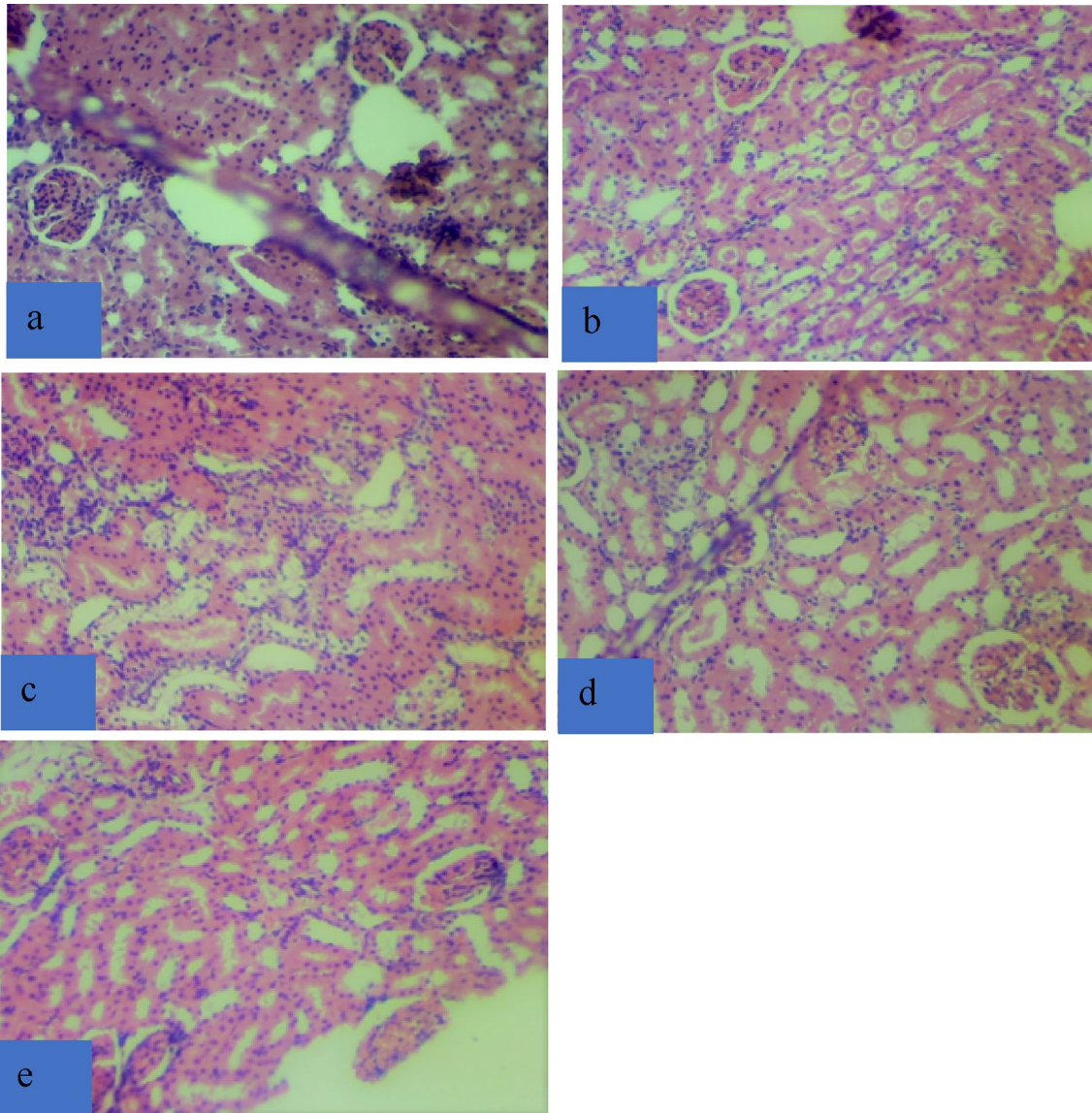Keys: SL 300 = *Securidaca longipedunculata* 300 mg/kgbwt, Fe$_2$O$_3$-NPs = iron oxide nanoparticle 300 mg/kgbwt, TC = total cholesterol

Plate 1 Histopathology of kidney section of rat treated with 300 mg/kgbwt of *S. longipedunculata* extract (**a**), 300 mg/kgbwt of Fe$_2$O$_3$-NPs (**b**), 5 mg/kgbwt of Glibenclamide (**c**), normal saline (**d**) and the negative control group (**d**) respectively showing renal tissue with preserved architecture composed of normal glomeruli tubules and interstitium. There are no features of acute or chronic damage in any of the group
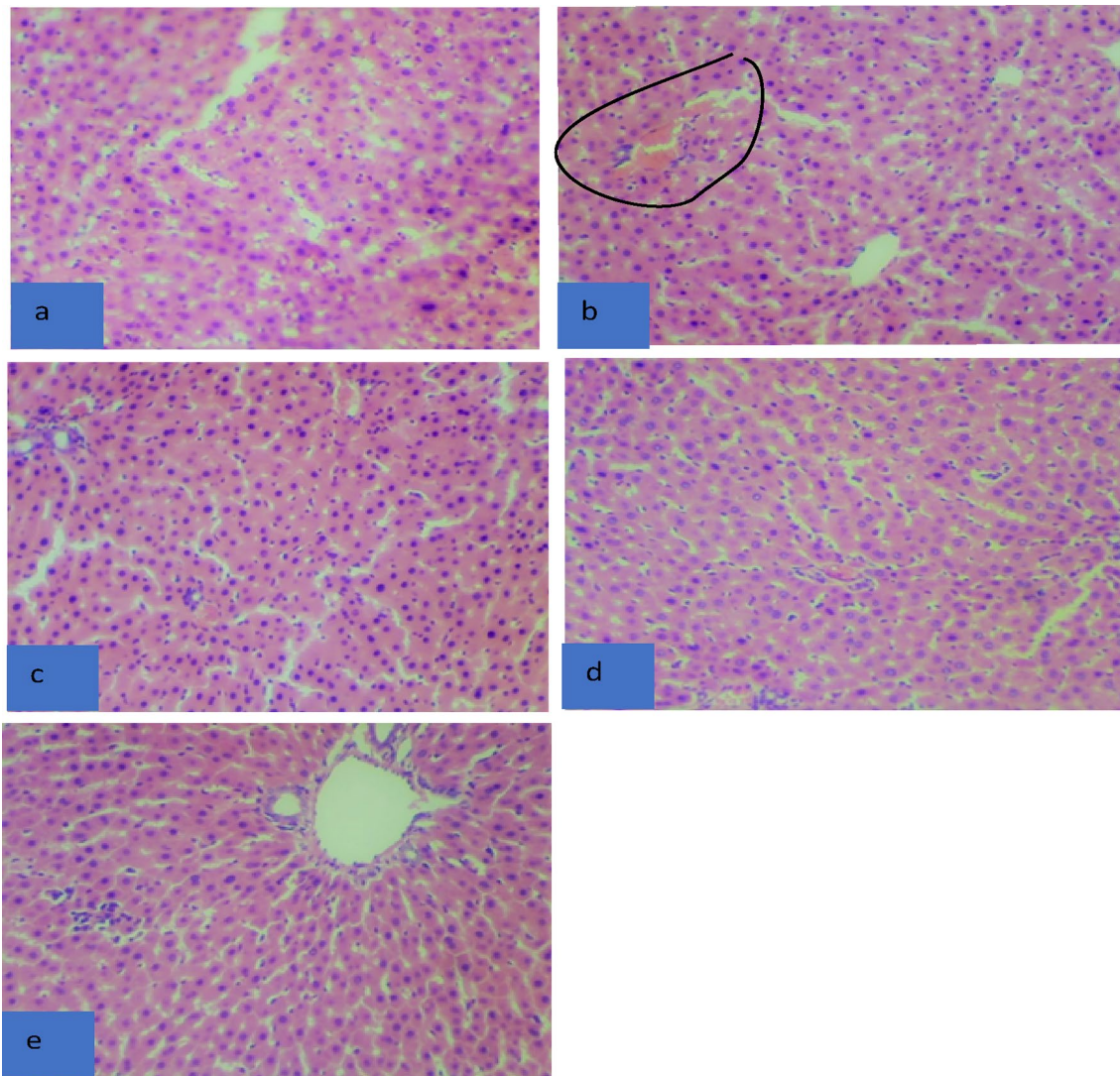
Plate 2 Histopathology of liver section of rat treated with 300 mg/kgbwt of *C. hindmannianus* extract (**a**), 300 mg/kgbwt of Fe$_2$O$_3$-NPs (**b**), 5 mg/kgbwt of Glibenclamide (**c**), normal saline (**d**) and the negative control group (**e**) respectively showing hepatic tissue with preserved architecture composed of cords of normal hepatocytes, nor- mal portal tracts and central vein. There are no features of acute or chronic damage in **a**, **c**, **d**, **e** except in rat treated with 300 mg/kgbwt of Fe$_2$O$_3$ nanoparticle which shows hepatic hemorrhage in the region highlighted above

diabetic rats with 300 mg/kgbwt showed significant increase ($p < 0.05$) in serum AST and ALP compared to the diabetic control group (Table 2). This report is contrary to the find-ings of Lamiaa et al. [42] who in his observed a decrease in these enzymes. The lipid profiles of rats treated with the extract and nanoparticles were also determined. The result shows an increase in the total cholesterol and triglycerides content of rats in the diabetic control group is significantly higher ($p < 0.05$) than those in the extract and nanoparticle treated group (Table 2). The Glibenclamide treated group shows no significant different ($p > 0.05$) in the HDL and LDL cholesterol level with the nanoparticle treated group but was significantly different ($p < 0.05$). The variation in the lipid profile between the extract treated group and nanoparti-cles may be linked to the phytochemical constituents present in the extract which aided the synthesis of the nanoparticle. For example, tannins and flavonoids found in the extract of the plant are known to have cholesterol lowering and athero-protective properties [52].

The histopathological study of the liver and kidney of the rats revealed a preserved histoarchitecture composed of cords of normal hepatocytes, normal portal tracts, central vein, normal glomeruli tubules and interstitium (Plate 1 and 2). There are no features of acute or chronic damage in any of the group hence the nanoparticle may be considered safe. This result however the outcome of Ali et al. [1] who

found an injury to the liver and kidney of rats treated with α-Fe_2O_3 nanoparticles. However, in their study the nanoparticles were coated with a functional polyethylene glycol. The observed differences may be due to the effect of chain length of polyethylene glycol on the nanoparticle biodistribution. Chain length of about 2 kDa increases the blood circulation time and decreases the opsonization of the nanoparticle by kuppfer cells and subsequently their localization in liver and toxicity.

Conclusion

The synthesis of α-Fe_2O_3 nanoparticles via green route was successfully carried out. Green synthesis is economically cheap, environmentally friendly and less toxic as it requires minimal chemical interactions and involved the use of biological materials such as the plant extract. The nanoparticle significantly lowered the blood glucose level of alloxan-induced diabetic rats. The size of the nanoparticles may also be attributed to the antidiabetic potentials of the nanoparticle since it has greater surface area and hence will be able to penetrated through the blood brain barriers to the target β-cells which may have been distorted by alloxan thereby lowering the blood glucose. Histological study if the liver and kidney of the rats shows no adverse sign of toxicity resulting from the daily intake of the nanoparticle. Thus, α-Fe_2O_3 nanoparticles may possess some antidiabetic potentials.

Declarations

Competing interests The authors have not disclosed any competing interests.

Ethics approval and consent to participate The study protocol was approved by the Ethical Committee of the Federal University Technology, Minna Nigeria and assigned number: 000022.

References

1. Ali, L.M.A., Shaker, S.A., Pinol, R., Millan, A., Hanafy, M.Y., Helmy, M.H., Kamel, M.A., Mahmoud, S.A.: Effect of superparamagnetic iron oxide nanoparticles on glucose homeostasis on type 2 diabetes experimental model. Life Sci. **245**, 117361 (2020)
2. Simcox, J.A., McClain, D.A.: Iron and diabetes risk. Cell Metab. **17**(3), 329–341 (2013). https://doi.org/10.1016/j.cmet.2013.02.007
3. Ovais, M., Khalil, A.T., Islam, N.U., Ahmad, I., Ayaz, M., Saravanan, M., Shinwari, Z.K., Mukherjee, S.: Role of plant phytochemicals and microbial enzymes inbiosynthesis of metallic nanoparticles. Appl. Microbiol. Biotechnol. **102**(16), 6799–6814 (2018). https://doi.org/10.1007/s00253-018-9146-7
4. El-Boubbou, K.: Magnetic iron oxide nanoparticles as drug carriers: preparation, conjugation and delivery. Nanomedicine **13**, 929–952 (2017)
5. Ponnaiah, S., Rajan, J.: A review on iron oxide nanoparticles and their biomedical applications. J. Supercond. Nov. Magn. **31**, 3397–3413 (2018)
6. Demirer, G.S., Okur, A.C., Kizilel, S.: Synthesis and design of biologically inspired biocompatible iron oxide nanoparticles for biomedical applications. J. Mater. Chem. B **3**, 7831–7849 (2015)
7. Parka, J., Kadasala, N.R., Abouelmagd, S.A., Castanares, M.A., Collins, D.S., Wei, A., Yeo, Y.: Polymer–iron oxide composite nanoparticles for EPR-independent drug delivery. Biomaterials **101**, 285–295 (2016)
8. Banerji, B., Pramanik, S.K., Mandal, S., Maiti, N.C., Chaudhuri, K.: Synthesis, characterization and cytotoxicity study of magnetic (Fe_3O_4) nanoparticles and their drug conjugate. RSC Adv. **2**, 2493–2497 (2012)
9. Vasantharaj, S., Sathiyavimal, S., Senthilkumar, P., LewisOscar, F., Pugazhendhi, A.: Biosynthesis of iron oxide nanoparticles using leaf extract of *Ruellia tuberosa*: antimicrobial properties and their applications in photocatalytic degradation. J. Photochem. Photobiol. B Biol. **192**, 74–82 (2019)
10. Devi HS, Boda MA, Shah MA, Parveen S, Wani AH.: Green synthesis of iron oxide nanoparticles using *Platanus orientalis* leaf extract for antifungal activity. Green Process. Synth. **8**(1), 38–45 (2019)
11. Muthukumar, H., Mohammed, S.N., Chandrasekaran, N.I., Sekar, A.D., Pugazhendhi, A., Matheswaran, M.: Effect of iron doped zinc oxide nanoparticles coating in the anode on current generation in microbial electrochemical cells. Int. J. Hydrogen Energy **44**, 2407–2416 (2019)
12. Ahmed, E.M.: Hydrogel: preparation, characterization, and applications: a review. J. Adv. Res. **6**(2), 105–121 (2015)
13. Khalil, A.T., Ovais, M., Ullah, I., Ali, M., Shinwari, Z.K., Maaza, M.: Biosynthesis of iron oxide (Fe_2O_3) nanoparticles via aqueous extracts of *Sageretia thea* (Osbeck.) and their pharmacognostic properties. Green Chem. Lett. Rev. **10**, 186–201 (2017)
14. Ovais, M., Khalil, A.T., Raza, A., Khan, M.A., Ahmad, I., Islam, N.U., Saravanan, M., Ubaid, M.F., Ali, M., Shinwari, Z.K.: Green synthesis of silver nanoparticles via plant extracts: beginning a new era in cancer theranostics. Nanomedicine **12**, 3157–3177 (2016)
15. Khalil, A.T., Ovais, M., Ullah, I., Ali, M., Shinwari, Z.K., Hassan, D., Maaza, M.: *Sageretia thea* (Osbeck.) modulated biosynthesis of NiO nanoparticles and their in vitro pharmacognostic, antioxidant and cytotoxic potential. Artif. Cells Nanomed. Biotechnol. **46**, 1–15 (2017). https://doi.org/10.1080/21691401.2017.1345928
16. Khalil, A.T., Ovais, M., Ullah, I., Ali, M., Shinwari, Z.K., Khamlich, S., Maaza, M.: *Sageretia thea* (Osbeck.) mediated synthesis of zinc oxide nanoparticles and its biological applications. Nanomedicine **12**, 1767–1789 (2017)
17. Ovais, M., Raza, A., Naz, S., Islam, N.U., Khalil, A.T., Ali, S., Khan, M.A., Shinwari, Z.K.: Current state and prospects of the phytosynthesized colloidal gold nanoparticles and their applications in cancer theranostics. Appl. Microbiol. Biotechnol. **101**, 3551–3565 (2017)
18. Kasithevar, M., Saravanan, M., Prakash, P., Kumar, H., Ovais, M., Barabadi, H., Shinwari, Z.K.: Green synthesis of silver nanoparticles using *Alysicarpus monilifer* leaf extract and its antibacterial

activity against MRSA and CoNS isolates in HIV patients. J. Interdiscip. Nanomed. **2**, 131–141 (2017)

19. Khan, M.A., Raza, A., Ovais, M., Sohail, M.F., Ali, S.: Current state and prospects of nano-delivery systems for sorafenib. Int. J. Polym. Mater. (2018). https://doi.org/10.1080/00914037.2018. 1429434

20. Alkaladi, A., Abdelazim, A.M., Afifi, M.: Antidiabetic activity of zinc oxide and silver nanoparticles on streptozotocin-induced diabetic rats. Int. J. Mol. Sci. **15**, 2015–2023 (2015)

21. Shaheen, T.I., El-Naggar, M.E., Hussein, J.S., El-Bana, M., Emara, E., El-Khayat, Z.: Antidiabetic assessment; in vivo study of gold and core–shell silver–gold nanoparticles on streptozotocin-induced diabetic rats. Biomed. Pharmacother. **83**, 865–887 (2016)

22. Sharifi, S., Daghighi, S., Motazacker, M.M., Badlou, B., Sanjabi, B., Akbarkhanzadeh, A.: Superparamagnetic iron oxide nanoparticles alter expression of obesity and T2 associated risk genes in human adipocytes. Sci. Rep. **3**, 2173 (2013)

23. Tshisikhawe M.P, Baloyi O, Maanda HL-M.: Ecología poblacional de Securidaca longepedunculata Fresen. en la Reserva Natural Nylsvley, Provincia Limpopo, Sudáfric. Phyton (Buenos Aires) **81**, 51–58 (2012)

24. Tikisa, T., Abdissa, D., Abdissa, N.: Chemical constituents of *Securidaca longipedunculata* root bark and evaluation of their antibacterial activities. Ethiop. J. Educ. Sci. **14**, 2 (2019)

25. Mongalo, N.I., McGaw, L.J., Finnie, J.F., Van Staden, J.: *Securidaca longipedunculata* Fresen (Polygalaceae): a review of its ethnomedicinal uses, phytochemistry, pharmacological properties and toxicology. J. Ethnopharmacol. **165**, 215–226 (2015)

26. Simeon, K.A., ImohImeh, J., Gbola, O.: Plants in respiratory disorders I antiasthmatics, a review. Br. J. Pharm. Res. **16**, 1–22 (2017)

27. Keay, R.W.J., Onochie, C.F.A., Stanfield, D.P.: Nigerian trees. Department of Forest Research Publishers, Ibadan (1964)

28. Ejikeme, C.M., Ezeonu, C.S., Eboatu, A.N.: Determination of physical and phytochemical constituents of some tropical timbers indigenous to Niger Delta Area of Nigeria. Eur. Sci. J. **10**(18), 247–270 (2014)

29. Hikino, H., Kiso, Y., Wagner, H., Fiebig, M.: Antihepatotoxic actions of flavonolignans from *Silybum marianum* fruits. Planta Med. **50**(3), 248–250 (1984)

30. Bibi, I., Nazar, N., Ata, S., Sultan, M., Ali, A., Abbas, A., Jilani, K., Kamal, S., Sarim, F.M., Khan, I., Jalal, F., Iqbal, M.: Green synthesis of iron oxide nanoparticles using pomegranate seEDX extract and photocatalytic activity evaluation for the degradation of textile dye. J. Mater. Res. Technol. **8**(6), 6115–6124 (2019)

31. Ojiako, A.O., Chikezie, P.C., Ogbuji, C.A.: Histopathological studies of renal and hepatic tissues of hyperglycemic rats administered with traditional herbal formulations. Int. J. Green Pharm. **9**, 184–191 (2015)

32. Belayneh, Y.M., Birru, E.M., Ambikar, D.: Evaluation of hypoglycemic, antihyperglycemic and antihyperlipidemic activities of 80% methanolic seed extract of *Calpurnia aurea* (Ait.) Benth. (Fabaceae) in mice. J. Exp. Pharmacol. **11**, 73–83 (2019). https://doi.org/10.2147/JEP.S212206

33. Friedewald, W., Levy, R., Fredrickson, D.: Estimation of concentration of low-density lipoprotein in plasma, without use of the preparative ultracentrifuge. Clin. Chem. **18**, 499–502 (1972)

34. Oluba, O.M., Olusola, A.O., Eidangbe, G.O., Babatola, L.J., Onyeneke, E.C.: Modulation of lipoprotein cholesterol levels in *Plasmodium berghei* malarial infection by crude aqueous extract of *Ganoderma lucidum*. Cholesterol **6**, 53–63 (2012)

35. Burnstein, M.A., Sammaille, J.A.: rapid determination of cholesterol bound to A and B lipoprotein. Clin. Chem. Acta **5**, 601–609 (1960)

36. Bhuiyan, S.H., Miah, M.Y., Paul, S.C., Aka, T.D., Saha, O., Rahaman, M., Habiba, J.I.O., Ashaduzzaman, M.D: Green synthesis of iron oxide nanoparticle using *Carica papaya* leaf extract: application for photocatalytic degradation of remazol yellow RR dye and antibacterial activity. Heliyon (2020). https://doi.org/10.1016/j. heliyon.2020.e04603

37. Behera, S.S., Patra, J.K., Pramanik, K., Panda, N., Thatoi, H.: Characterization and evaluation of antibacterial activities of chemically synthesized iron oxide nanoparticles. World J. Nanosci. Eng. **2**, 196 (2012)

38. Fouad, D.F., Zhang, C., El-Didamony, H., Yingnan, L., Mekuria, T.D., Shah, A.H.: Improved size, morphology and crystallinity of hematite (α-Fe_2O_3) nanoparticles synthesized via the precipitation route using ferric sulfate precursor. Results Phys. **12**, 1253–1261 (2019). https://doi.org/10.1016/j.rinp.2019.01.005

39. Ahmmad, B., Leonard, K., Islam, S., Kurawaki, J., Muruganandham, M.: Green synthesis of mesoporous hematite (α-Fe_2O_3) nanoparticles and their photocatalytic activity. Adv. Powder Technol. **24**(1), 160–167 (2013)

40. Suresh, S., Karthikeyan, S., Jayamoorthy, K.: Effect of bulk and nano-Fe_2O_3 particles on peanut plant leaves studied by Fourier transform infrared spectral studies. J. Adv. Res. **7**, 739–747 (2016)

41. Lassoued, A., Lassoued, M.S., Dkhil, B., Ammar, S., Gadri, A.: Photocatalytic degradation of methylene blue dye by iron oxide (α-Fe_2O_3) nanoparticles under visible irradiation. J. Mater. Sci. Mater. Electron. **29**, 8142–8152 (2018)

42. Lamiaa, M.A.A., Sara, A.S., Rafael, P., Millan, A., Mervat, Y.H., Madiha, H.H., Maher, A.K., Shimaa, A.M.: Effect of superparamagnetic iron oxide nanoparticles on glucose homeostasis on type 2 diabetes experimental model. Life Sci. **245**, 117361 (2020)

43. Liu, J., Li, Q., Yang, Y., Ma, L.: Iron metabolism and type 2 diabetes mellitus: a meta-analysis and systematic review. J. Diabetes Investig. **11**, 946–955 (2020). https://doi.org/10.1111/jdi.13216

44. Carlos, A.R., Weis, S., Soares, M.P.: Cross-talk between iron and glucose metabolism in the establishment of disease tolerance. Front. Immunol. **9**, 2498 (2018). https://doi.org/10.3389/fimmu. 2018.02498

45. Bhardwaj, M., Yadav, P., Vashishth, D., Sharma, K., Kumar, A., Chahal, J., Dalal, S., Kataria, S.K.: A review on obesity management through natural compounds and a green nanomedicine-based approach. Molecules **26**(11), 3278 (2021)

46. Balan, K., Qing, W., Wang, Y., Liu, X., Palvannan, T., Wang, Y., Ma, F., Zhang, Y.: Antidiabetic activity of silver nanoparticles from green synthesis using *Lonicera japonica* leaf extract. RSC Adv. **6**(46), 40162–40168 (2016)

47. Najafabadi, R.E., Kazemipour, N., Esmaeili, A., Beheshti, S., Nazifi, S.: Quercetin prevents body weight loss due to the using of superparamagnetic iron oxide nanoparticles in rat. Adv. Biomed. Res. **7**(8), 14–17 (2018). https://doi.org/10.4103/abr.abr_141_17

48. Szalay, B., Tátrai, E., Nyírő, G., Vezér, T., Dura, G.: Potential toxic effects of iron oxide nanoparticles in in vivo and in vitro experiments. J. Appl. Toxicol. **32**, 446–453 (2012)

49. Zhu, M.T., Wang, Y., Feng, W.Y., Wang, B., Wang, M., Ouyang, H.: Oxidative stress and apoptosis induced by iron oxide nanoparticles in cultured human umbilical endothelial cells. J. Nanosci. Nanotechnol. **10**, 8584–8590 (2012)

50. Khan, M.I., Mohammad, A., Patil, G., Naqvi, S.A., Chauhan, L.K., Ahmad, I.: Induction of ROS, mitochondrial damage and autophagy in lung epithelial cancer cells by iron oxide nanoparticles. Biomaterials **33**, 1477–1488 (2012)

51. Alarifi, S., Ali, D., Alkahtani, S., Alhader, M.S.: Iron oxide nanoparticles induce oxidative stress, DNA damage, and caspase activation in the human breast cancer cell line. Biol. Trace Elem. Res. **159**, 416–424 (2014)

52. Ikewuchi, J.C., Onyeike, E.N., Uwakwe, A.A., Ikewuchi, C.C.: Effect of aqueous extract of the leaves of *Acalypha wilkesiana*

'Godseffiana' Muell Arg (Euphorbiaceae) on the hematology, plasma biochemistry and ocular indices of oxidative stress in alloxan induced diabetic rats. J. Ethnopharmacol. **137**(3), 1415–1424 (2017). https://doi.org/10.1016/j.jep.2011.08.015

Publisher's Note Springer Nature remains neutral with regard to jurisdictional claims in published maps and institutional affiliations.